Available online at www.sciencedirect.com
SCIENCE DIRECT®
ELSEVIER
Journal of Magnetism and Magnetic Materials 277 (2004) 144–152
Journal of magnetism and magnetic materials
www.elsevier.com/locate/jmmm

Structural and magnetic properties of $Ni_{81}Fe_{19}$/Zr multilayers

A. Biondo[a,c,*], V.P. Nascimento[a], H. Lassri[b], E.C. Passamani[c], M.A. Morales[a], A. Mello[a], R.S. de Biasi[d], E. Baggio-Saitovitch[a]

[a] *CME Centro Brasileiro de Pesquisas Físicas, Rua Dr. Xavier Sigaud 150 Urca, Rio de Janeiro, RJ 22290-180, Brazil*
[b] *Laboratoire de Physique des Matériaux et de Micro-électronique, Faculté des Sciences Ain Chock, Université Hassan II, B.P. 5366 Mâarif, Route d'El Jadida, Km-8, Casablanca, Morocco*
[c] *Universidade Federal do Espírito Santo, Departamento de Física, Vitória, ES 29060-900, Brazil*
[d] *Instituto Militar de Engenharia, Departamento de Engenharia Mecânica e de Materiais, Rio de Janeiro, RJ 22290-270, Brazil*

Received 9 September 2003; received in revised form 9 October 2003

Abstract

Structural and magnetic properties of $Ni_{81}Fe_{19}$/Zr multilayers, prepared by DC magnetron sputtering, were studied using X-ray diffraction, ferromagnetic resonance and magnetization. Low-angle X-ray diffraction results are typical of a modulated structure, while high-angle data suggest that the $Ni_{81}Fe_{19}$ layers can have amorphous or crystalline structure depending on the thickness. Saturation magnetization increases significantly with thickness of the $Ni_{81}Fe_{19}$ layers, an effect attributed to the increase in the bulk-to-interface ratio. In a sample where the thickness of the $Ni_{81}Fe_{19}$ layers is 40 Å, the FMR spectrum, with the magnetic field perpendicular to the film plane, displays a spin wave feature, with odd and even modes. Two surface modes are also observed, suggesting that unpinning occurs at both interfaces of the $Ni_{81}Fe_{19}$ layers. For $Ni_{81}Fe_{19}$ layers thicker than 40 Å, FMR and magnetization data show a surface anisotropy constant (K_S) of about $-0.32\,erg/cm^2$, which is an indication that the magnetic moment in the $Ni_{81}Fe_{19}$ layers is confined to the film plane.

PACS: 73.21.A; 75.30.G; 75.30.D

Keywords: Multilayer; Magnetic anisotropy; Spin waves

1. Introduction

Magnetic multilayers have attracted great attention in recent years due to their interesting physical properties and potential technological applications. In the case of some multilayers, such as Fe/Cr, Co/Cu and $Ni_{81}Fe_{19}$/Cu, the main focus has been on the giant magnetoresistance effect (GMR) [1–3], but in others, the goal has been the investigation of the magnetic properties at the interface regions, such as interfacial anisotropy [4,5] and interfacial roughness [6].

Multilayers with $Ni_{81}Fe_{19}$ layers have been intensively studied since the discovery of their GMR effect [2]. In addition to magnetoresistance

*Corresponding author. CME Centro Brasileiro de Pesquisas Físicas, Rua Dr. Xavier Sigaud 150 Urca, Rio de Janeiro, RJ 22290-180, Brazil. Tel.: +552121417184; fax: +552121417540.
E-mail address: biondo@cbpf.br (A. Biondo).

0304-8853/$ - see front matter © 2003 Elsevier B.V. All rights reserved.
doi:10.1016/j.jmmm.2003.10.019

(MR), these multilayers exhibit properties that may lead to applications in magnetic sensing and magnetic recording [7,8].

In this work, we report some results on $Ni_{81}Fe_{19}$/Zr multilayers. Amorphous NiFeZr displays interesting magnetic properties but is seldom observed in thin films [9,10]. On the other hand, $Ni_{81}Fe_{19}$/Zr multilayers should be relatively easy to prepare. Thus, counting with the possibility of studying the structure and magnetism of the $Ni_{81}Fe_{19}$ phase at the interfaces of Zr layers, we prepared two series of $Ni_{81}Fe_{19}$/Zr multilayers, varying the thickness of the Zr and $Ni_{81}Fe_{19}$ layers. X-ray diffraction, magnetization, ferromagnetic resonance (FMR) and magnetotransport measurements were used to investigate the structural and magnetic properties of these multilayers.

2. Experimental procedure

$Ni_{81}Fe_{19}$ and Zr single layers and Si/Zr/$[Ni_{81}Fe_{19}/Zr]_n$/Zr multilayers were prepared by DC magnetron sputtering, using high-purity $Ni_{81}Fe_{19}$ and Zr targets. The pressure in the chamber before deposition was roughly 6×10^{-8} Torr, while the gas (ultra-high-purity argon) pressure was kept constant, at 2×10^{-3} Torr, using feedback gauge valve control. The DC power was 80 W. Films were deposited onto a water-cooled Si (0 0 1) substrate kept at a temperature of 20°C. The $Ni_{81}Fe_{19}$/Zr multilayers were prepared in two series. Series I, with the thickness of the $Ni_{81}Fe_{19}$ layers (t_{NiFe}) varying from 20 to 120 Å, keeping the Zr thickness (t_{Zr}) at 15 Å. In series II, t_{NiFe} was 30 Å while t_{Zr} varied from 3 to 20 Å. In series I, the number of periods (n) varied from 10 (for $t_{NiFe}=120$ Å) to 20 (for $t_{NiFe}=20$ Å), while for series II $n=15$. In both series, Zr buffer and capping layers of 100 and 50 Å, respectively, were used.

Low-angle X-ray diffraction (LXRD) measurements were done to check the artificial periodic structure and layer thickness of the films. The $Ni_{81}Fe_{19}$ (2.9 Å/s) and Zr (1.7 Å/s) deposition rates were calculated dividing the single layers thicknesses by their respective deposition times. High-angle X-ray diffraction (HXRD) measurements were made to investigate the atomic structures of the $Ni_{81}Fe_{19}$ and Zr layers in the multilayers.

Magnetization measurements were made using a vibrating sample magnetometer (VSM) with precision better than 5% to obtain the saturation magnetization M_S.

The AC resistivity was measured as a function of the applied field using the standard four-probe configuration, with the applied field perpendicular to the current, to investigate the film MR, which was defined as

$$\Delta R/R=(R_0-R_S)/R_S, \tag{1}$$

where R_S is the sample resistance in the presence of an applied field and R_0 is the resistance at zero field.

FMR measurements were performed at 300 K and 9.59 GHz for the samples of series I. The effective magnetization M_{eff} and the g factor were calculated from FMR spectra taken with the static magnetic field perpendicular ($H_\perp$) and parallel ($H_\parallel$) to the film plane. From the H_K versus $1/t_{NiFe}$ curve, the superficial (K_S) and volumetric (K_U) anisotropy constants of the $Ni_{81}Fe_{19}$ layer were estimated.

3. Results and discussion

The LXRD patterns of all multilayers in series I and II show well-defined reflectivity peaks superimposed with small oscillations between the peaks (see Fig. 1). The pronounced peaks in the LXRD patterns are a clear indication for the well-established artificial modulated structure of the $Ni_{81}Fe_{19}$/Zr samples. The small oscillations between the pronounced peaks are related to good quality of the interface (low roughness). However, evidence of a periodic distribution was observed in some of the samples, specifically in $Ni_{81}Fe_{19}$(30 Å)/Zr (15 Å) multilayer (Fig. 1(b)). It can be caused by atomic diffusion processes through the interfaces, forming layers with different shapes and consequently no regular thickness. This topic will be clarified later. One was able to estimate the periods of the multilayers and the values, obtained from the peak positions, are in reasonable

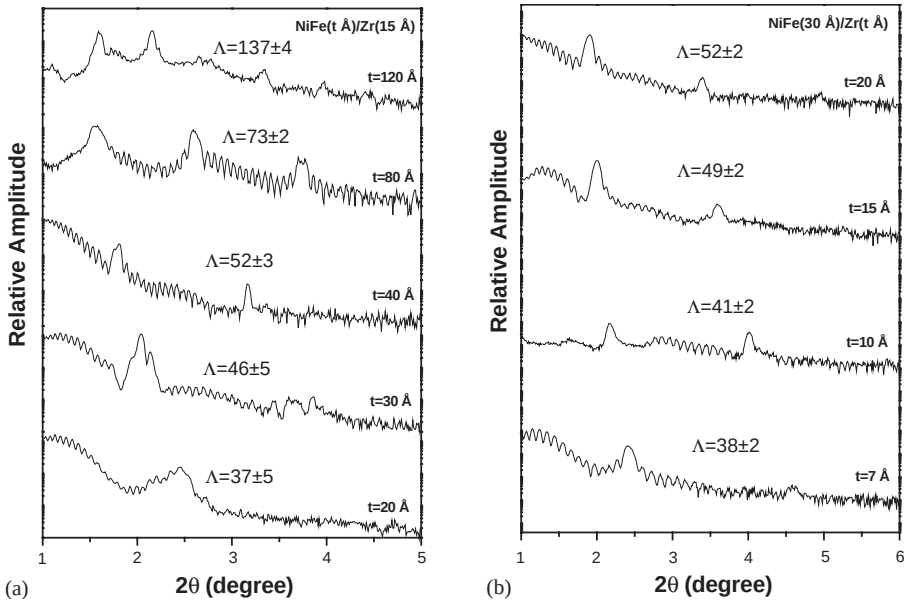

Fig. 1. LXRD patterns of series I (a), and series II samples (b) of NiFe/Zr multilayers.

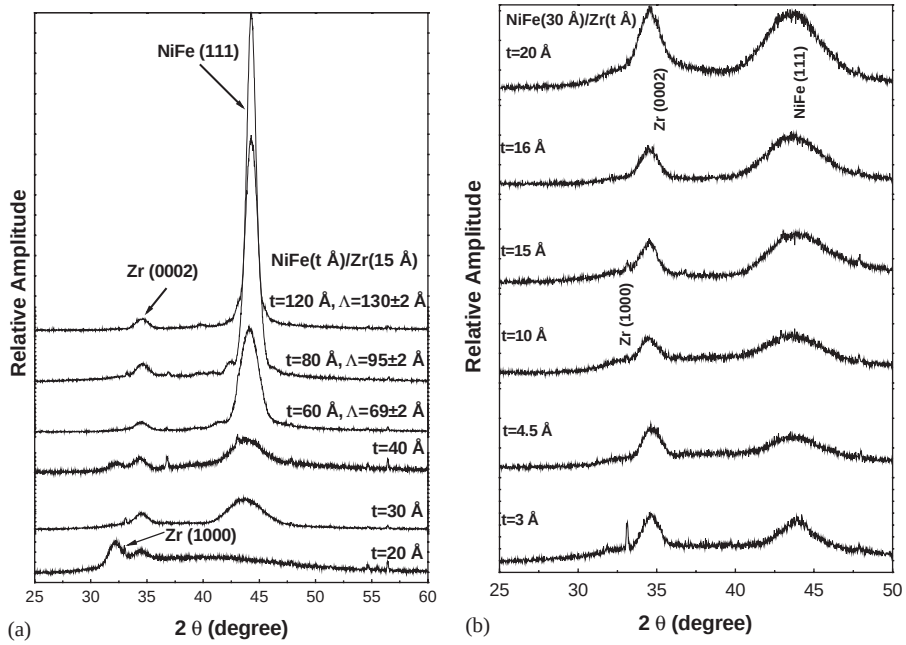

Fig. 2. HXRD patterns of series I (a), and series II samples (b) of NiFe/Zr multilayers.

agreement with the nominal ones, as indicated in Figs. 1(a) and (b).

The HXRD patterns for series I and II are shown in Figs. 2(a) and (b), respectively. In general, these HXRD patterns show one Bragg peak beyond the FCC-$Ni_{81}Fe_{19}$ diffraction and two Bragg peaks related to the HCP-Zr. A sharp peak that sometimes appears at $2\theta = 33^\circ$ is due to

the silicon substrate. The coherence lengths of the peaks were estimated using the Scherrer formula [11,12]. Therefore, considering that: (a) the coherence length and the intensity of Zr (1 0 0 0) and Zr (0 0 0 2) peaks of both series are independent of Zr spacing layers thickness (see Table 1); (b) the HXRD pattern of the multilayer with the lowest Zr spacer also presents the related HCP peaks and (c) HCP-Zr detached crystalline peaks becomes to appear in the diffraction patterns of Ni/Zr multilayers for Zr layers with more than 19 atomic planes (about 98 Å) [13], one may suggest that the HCP-Zr peaks, present in the HXRD patterns of our multilayers, are related to the buffer and/or capping layers. In addition, in all samples, the coherence lengths extracted from the peaks related to the $Ni_{81}Fe_{19}$ layers are not higher than t_{NiFe}. Then, one can be sure that these peak positions are corresponding to the out-of-plane interatomic distance of $Ni_{81}Fe_{19}$ and only the NiFe layers contribute expressively to the $Ni_{81}Fe_{19}$/Zr superlattice crystallinity. However, one has to emphasize that for the film with $t_{NiFe} = 20$ Å (series I) the HXRD pattern does not show the presence of the $Ni_{81}Fe_{19}$ Bragg peak. This can be explained by the large size mismatch between the constituents and intermixing during the deposition producing disordered interfaces, which extend several atomic planes on either side of interfaces. Summarizing, the $Ni_{81}Fe_{19}$/Zr superlattices, with low t_{NiFe}, could be entirely amorphous, as indicated by the broad Bragg peak observed in the X-ray patterns. As t_{NiFe} increases, the central portion of the layers will be crystalline. For the sample with $t_{NiFe} = 30$ Å the broad peak close to the (1 1 1) $Ni_{81}Fe_{19}$ Bragg diffraction is slightly shifted to lower angles. In principle, the broadening effect can be attributed to the $Ni_{81}Fe_{19}$ thickness effect, as estimated using the Scherrer formula. However, the observed shift is real and may be a consequence of (i) an amorphous NiFeZr alloy formed at the interfaces or (ii) a strained $Ni_{81}Fe_{19}$ structure grown, on the top of the Zr layer, with lattice parameter larger than that of bulk $Ni_{81}Fe_{19}$ phase. Both effects may be enhanced when the $Ni_{81}Fe_{19}$ thickness is relatively low. It can also be seen in the HXRD of series I that increasing t_{NiFe}, the $Ni_{81}Fe_{19}$ peak related to (1 1 1) plane shifts in the direction of the bulk (1 1 1) angular position of the $Ni_{81}Fe_{19}$ phase. Indeed, for films with $t_{NiFe} > 80$ Å, the (1 1 1) peak has the same angular position as the bulk $Ni_{81}Fe_{19}$ reflection. Thus, one may say that increasing t_{NiFe}, the interface contribution becomes less evident compared with the contribution of the inner part of the $Ni_{81}Fe_{19}$ layer, resulting in a global observation that is governed by the bulk $Ni_{81}Fe_{19}$ phase. Apparently, the $Ni_{81}Fe_{19}$ layers have a relaxed lattice structure, as suggested by the shift of (1 1 1) peak to bulk angular position.

Table 1
Coherence lengths L_{NiFe}, L_{Zr} (1 0 0 0) and L_{Zr} (0 0 0 2) calculated from the $Ni_{81}Fe_{19}$ (1 1 1), Zr (1 0 0 0) and Zr (0 0 0 2) Bragg peaks, using the Scherrer formula

Multilayer	Period (nominal) (Å)	L_{NiFe} (1 1 1) (Å)	L_{Zr} (1 0 0 0) (Å)	L_{Zr} (0 0 0 2) (Å)
$Ni_{81}Fe_{19}$(20 Å)/Zr(15 Å)	35	—	40±1	56±1
$Ni_{81}Fe_{19}$(30 Å)/Zr(15 Å)	45	29±1		62±1
$Ni_{81}Fe_{19}$(40 Å)/Zr(15 Å)	55	31±1	43±1	55±1
$Ni_{81}Fe_{19}$(60 Å)/Zr(15 Å)	75	51±1	—	75±1
$Ni_{81}Fe_{19}$(80 Å)/Zr(15 Å)	95	75±1	—	75±1
$Ni_{81}Fe_{19}$(120 Å)/Zr(15 Å)	135	115±1	—	54±1
$Ni_{81}Fe_{19}$(30 Å)/Zr(3 Å)	33	31±1	—	78±1
$Ni_{81}Fe_{19}$(30 Å)/Zr(5 Å)	35	27±1	—	72±1
$Ni_{81}Fe_{19}$(30 Å)/Zr(7 Å)	37	24±1	—	—
$Ni_{81}Fe_{19}$(30 Å)/Zr(9 Å)	39	18±1	—	31±1
$Ni_{81}Fe_{19}$(30 Å)/Zr(10 Å)	40	16±1	—	57±1
$Ni_{81}Fe_{19}$(30 Å)/Zr(15 Å)	45	24±1	—	77±1
$Ni_{81}Fe_{19}$(30 Å)/Zr(16 Å)	46	17±1	—	59±1
$Ni_{81}Fe_{19}$(30 Å)/Zr(20 Å)	50	26±1	—	53±1

Another important point to be stressed is that close to the $Ni_{81}Fe_{19}$ peaks, the HXRD patterns show the satellite peaks characteristic of superstructure with a $Ni_{81}Fe_{19}$ (1 1 1) fiber texture. The periods deduced from the low-angle Bragg peaks and from the satellite peaks are in good agreement and the values are specified in Fig. 2(a).

Table 2 displays the saturation magnetization per unit volume of the multilayers as a function of the thickness of the magnetic layers. The magnetization saturation values increase with the magnetic layer thickness. This could be explained in terms of a magnetically dead layer contribution in both interface sides of the $Ni_{81}Fe_{19}$ layers due to alloying effects. It is known from the dead layer model [14] that the magnetization of multilayer (M) can be expressed as

$$M = M_0(1 - t_0/t_{NiFe}), \quad (2)$$

where M_0 is the bulk $Ni_{81}Fe_{19}$ value and $t_0/2$ is the dead layer thickness at each interface. The thickness of such a dead layer can be estimated by plotting the product Mt_{NiFe} as a function of t_{NiFe}, as shown in Fig. 3. The slope of this curve corresponds to a magnetization value of $(8.5 \pm 0.3) \times 10^2$ emu/cm^3, while its x-intercept gives a t_0 (dead layer thickness) of (19.3 ± 0.2) Å.

Fig. 4 shows the room-temperature MR of series I (Fig. 4(a)) and series II (Fig. 4(b)) as a function of the t_{NiFe} and t_{Zr}, respectively. In series I, the MR curve displays one maximum of about 1.8% at $t_{NiFe} = 80$ Å and the MR values practically vanished for t_{NiFe} up to 40 Å. Also, the MR peaks of series II show amplitudes close to those observed in series I for $t_{NiFe} \leqslant 40$ Å; the two peaks are of 0.4% at $t_{Zr} = 7$ Å and 0.3% at $t_{Zr} = 15$ Å.

Since it is well known that the MR values for amorphous materials are small in magnitude and combining the results of X-ray, magnetization and MR one can suggest that for low t_{NiFe} the main contribution is due to an amorphous phase formed

Table 2
Magnetization per unit volume of series I samples

t_{NiFe} (Å)	$4\pi M_S$ (G)
20	1449
30	4788
40	5049
60	6590
80	7700
120	9215

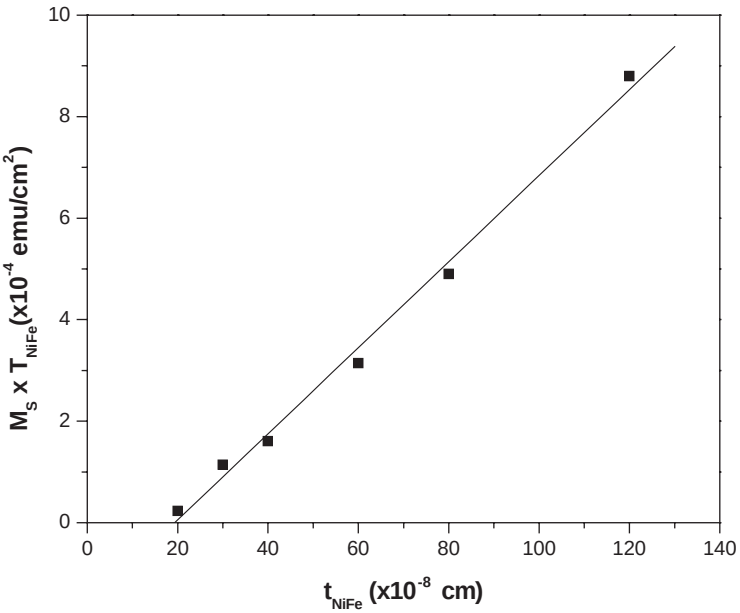

Fig. 3. Dependence of the product M_S (at 300 K)t_{NiFe} on the $Ni_{81}Fe_{19}$ layer thickness.

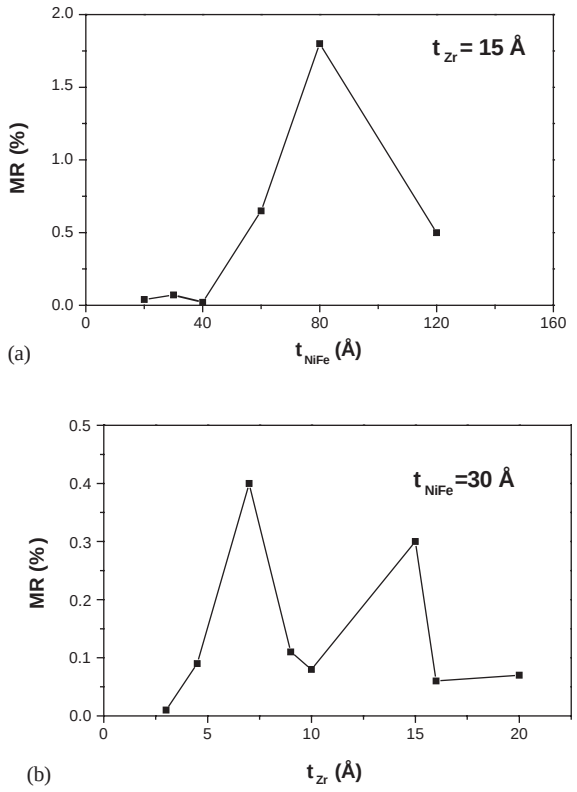

Fig. 4. MR, measured at 300 K, as a function of t_{NiFe} (series I samples) and t_{Zr} (series II samples).

by the diffusion of Zr into the $Ni_{81}Fe_{19}$ layer. The latter argument is based on the observation of (1 1 1) Bragg peak of the $Ni_{81}Fe_{19}$ phase.

Typical FMR spectra for series I are shown in Fig. 5. For $t_{NiFe} \geqslant 60$ Å, a linear resonance mode ($k = 0$) is observed in the multilayers for applied magnetic fields, both parallel ($H_{\|}$) and perpendicular ($H_{\perp}$) to the film plane. In the perpendicular case, for higher resonance fields, a surface spin wave mode appears as an extra peak, indicating that an unpinning of the spins occurs at one surface [15,16]. The absence of multipeak resonance can be explained by a situation where the spins of both surfaces have a natural freedom (surface parameters equal to 1), where only one resonance absorption (uniform mode) would be observed. However, it does not explain the surface mode existence. Thus, the absence of bulk modes and the presence of one surface mode could be explained by a situation where the spins of both surfaces have a pinning condition close to the natural freedom (surface parameters near 1) and one of the surface parameters has to be slightly greater than 1 (unpinning of the surface spins) to excite the surface mode forming a quasi-antisymmetric surface state [16]. For $t_{NiFe} = 40$ Å, in the $H_{\|}$ case, only one absorption mode (linear mode) is observed; however, in the $H_{\perp}$ case, one spin wave spectrum with both odd- and even-numbered modes can be seen; indicating that pinning in this film is asymmetrical [16] at the two surfaces of the magnetic layer. In addition, the intensity of the odd modes is higher than of the even modes; this effect appears when the same situations occur at both surfaces, either pinning or unpinning [16]. This ambiguity is removed by the presence of two surface modes observed in this spectrum, for higher fields, which shows that both surface parameters are greater than 1 and consequently the spins of both surfaces of the magnetic layer are unpinning [16].

Fig. 6 shows the dependence of the spin wave resonance field H_{res} on the spin wave numbers n; the curve has the usual linear behavior when the spin wave field positions are plotted against n^2. For t_{NiFe} equal to 20 and 30 Å, three and two, respectively, resonance peaks with low intensity appear in the spectra for $H_{\|}$ and $H_{\perp}$. The presence of more than one resonance absorption mode may be associated with magnetic inhomogeneities present in the layer [17], which, according to X-ray and magnetization are due to Zr atoms diffusing into the $Ni_{81}Fe_{19}$ layers and forming an amorphous NiFeZr phase.

In order to obtain information about the magnetic properties of the FCC-$Ni_{81}Fe_{19}$ layer in series I ($t_{NiFe} \geqslant 40$ Å), the FMR spectra were analyzed taking into account the strongest mode. Thus, one calculated the constants $4\pi M_{eff}$ and the g factor using the expressions proposed in the literature [18–20], where the resonance field H_{res} corresponds to the uniform mode in a single-layer film:

For the perpendicular geometry, one has

$$(\omega/\gamma)_{\perp} = H_{\perp} - 4\pi M_{eff}. \quad (3)$$

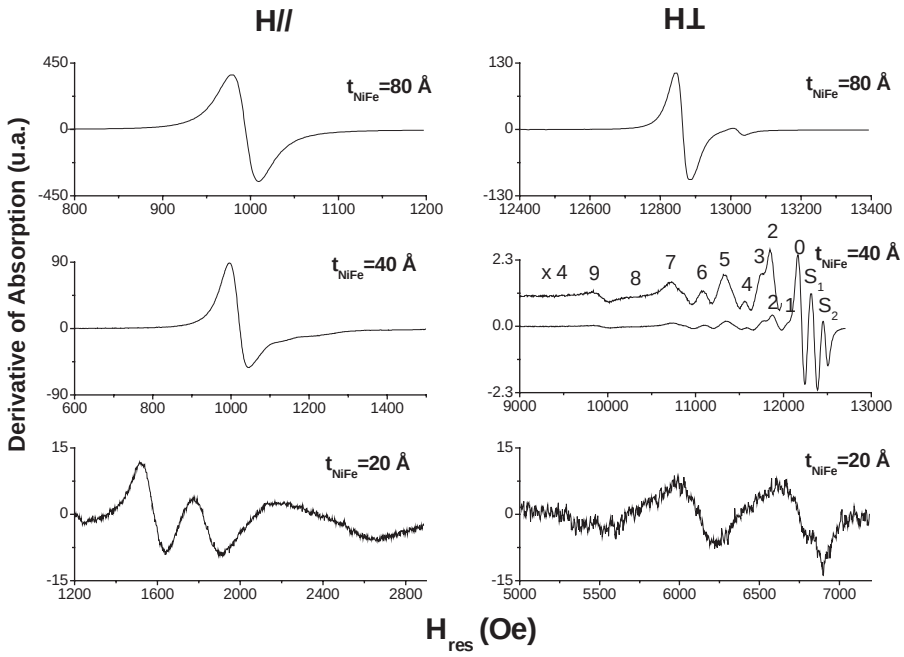

Fig. 5. FMR spectra of series I samples recorded at 300 K under applied fields parallel ($H_{\parallel}$) and perpendicular ($H_{\perp}$) to the film plane.

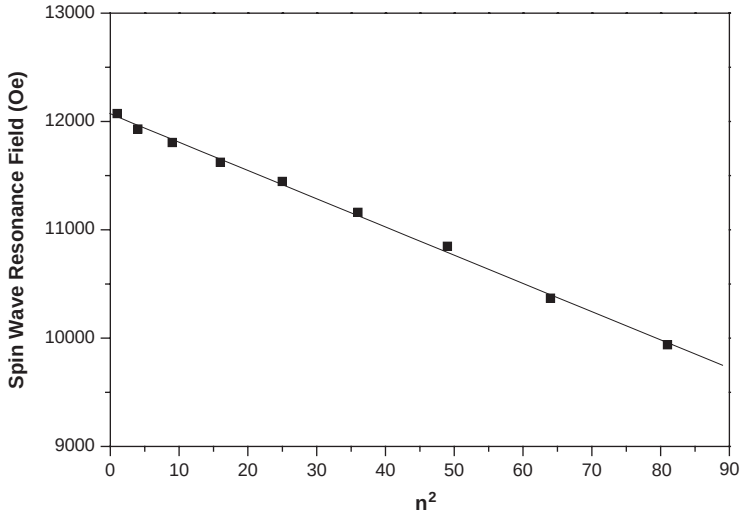

Fig. 6. SWR field position for a NiFe (40 Å)/Zr(15 Å) multilayer as a function of n^2.

For parallel geometry, one has

$$(\omega/\gamma)_{\parallel}^2 = H_{\parallel}(H_{\parallel} + 4\,\pi\,M_{\mathrm{eff}}). \quad (4)$$

Table 3 shows the values of $4\pi M_{\mathrm{eff}}$ and g for series I.

According to previous studies [5,21], the interface magnetic anisotropy of multilayers can be derived from the dependence of the perpendicular anisotropy field on the thickness of the magnetic layer, if the interface anisotropy essentially

Table 3
Effective magnetization and g factor of series I samples

t_{NiFe} (Å)	$4\pi M_{eff}$ (G)	g
20	5098	2.09
30	7590	2.10
40	8911	2.10
60	9133	2.11
80	9615	2.11
120	9995	2.11

enhances the first-order anisotropy energy K_1. Thus the perpendicular anisotropy field (excluding the demagnetization term) can be written as

$$H_K = H_U + 2H_S/t_{NiFe}, \quad (5)$$

i.e.,

$$H_K = 4\pi M_S - 4\pi M_{eff} = H_U + 2H_S/t_{NiFe}. \quad (6)$$

The perpendicular anisotropy field $H_K = 2K_1/M_S$ includes two terms, a volume anisotropy $H_U = 2K_U/M_S$ and a surface-induced anisotropy $H_S = 2K_S/M_S$.

When the demagnetization energy is taken into account, one may write Eq. (6) as

$$K_{eff} = K_V + 2K_S/t_{NiFe}, \quad (7)$$

where

$$K_V = K_U - 2\pi M_S^2, \quad K_{eff} = K_1 - 2\pi M_S^2. \quad (8)$$

K_{eff} and K_V are the effective perpendicular anisotropy energy and effective volume anisotropy energy, respectively (including the demagnetization energy).

Fig. 7 shows a plot of H_K as a function of $1/t_{NiFe}$. From the slope of the straight line, the value of the interface anisotropy constant K_S is found to be $K_S = (-0.32 \pm 0.01)\,erg/cm^2$. Also, by extrapolating the straight line to $1/t_{NiFe} = 0$, we obtain $H_U = 522\,Oe$ and $K_U = (1.9 \pm 0.5) \times 10^5\,erg/cm^3$.

In general, we assumed that the interface anisotropy energy constant K_s could be originated from several effects which change the surface spins at the interfaces, such as misfit strain anisotropy [4], surface roughness [6] and Néel anisotropy [22]. This assumption was considered in our samples for t_{NiFe} larger than 30 Å, where the Zr atoms diffused in the $Ni_{81}Fe_{19}$ layers is a minority fraction and one may suppose that the magnetic interface anisotropy is not drastically affected. The negative value of K_S may be an indication that the magnetic moments in the magnetic layer surface are confined to the film plane.

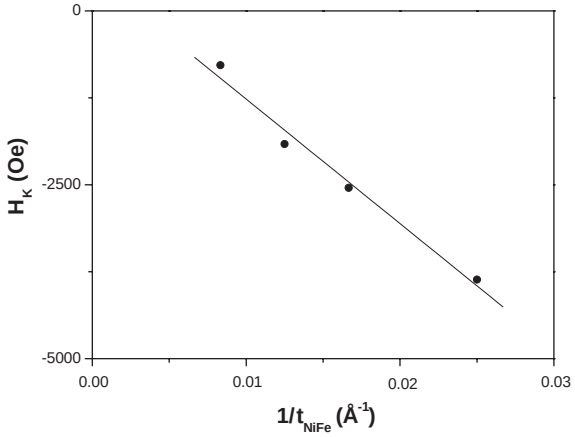

Fig. 7. Perpendicular anisotropy field (H_K) as a function of $1/t_{NiFe}$.

4. Conclusions

In this work, structural and magnetic properties of the $Ni_{81}Fe_{19}$/Zr multilayers have been studied by different experimental techniques. An amorphous NiFeZr phase is formed by the diffusion of Zr into the $Ni_{81}Fe_{19}$ layer. This phase shows soft magnetic properties similar to that of the FCC-$Ni_{81}Fe_{19}$ phase that constitutes the inner part of the magnetic layers. Also, as it is well known and we have shown, the room-temperature magnetic moment of the amorphous NiFeZr phase is smaller than that of the FCC-$Ni_{81}Fe_{19}$ phase. The magnetization ratio between the FCC-$Ni_{81}Fe_{19}$ and amorphous NiFeZr phases increases with t_{NiFe} and the saturation magnetization reaches the FCC-$Ni_{81}Fe_{19}$ bulk value for $t_{NiFe} > 80$ Å. For $t_{NiFe} = 40$ Å, FMR measurements show one spin wave resonance with both odd- and even-numbered modes. In addition, two surface modes are observed, indicating that there is unpinning at both surfaces of the magnetic layer.

The negative value of K_S may be an indication that the magnetic moments in the magnetic layer surface are confined to the film plane.

Acknowledgements

This work was supported by CNPq, CAPES–PICD/UFES, PCI-MCT and FAPERJ (Cientista do Nosso Estado Program). H. Lassri and E.C. Passamani thank PCI-MCT program for supporting their visit to CBPF. We thank A.Y. Takeuchi for the VSM measurements and J.P.D. Cavalcante for digitalizing the FMR spectra.

References

[1] M.N. Baibich, J.M. Broto, A. Fert, F. Nguyen Van Dau, F. Petroff, P. Eitenne, G. Creuzet, A. Frederich, J. Chazelas, Phys. Rev. Lett. 61 (1988) 2472.
[2] S.S. Parkin, Appl. Phys. Lett. 60 (1992) 512.
[3] A. Paul, T. Damm, D.E. Burgler, S. Stein, H. Kohlstedt, P. Grunberg, J. Magn. Magn. Mater. 15 (17) (2003) 2471.
[4] F.J.A. den Broeder, W. Hoving, P.J.H. Bloemen, J. Magn. Magn. Mater. 93 (1991) 562.
[5] U. Gradmann, J. Magn. Magn. Mater. 54–57 (1986) 733.
[6] P. Bruno, J. Appl. Phys. 64 (1988) 3153.
[7] R. Nakatani, T. Dei, T. Kobayashi, Y. Sugita, IEEE Trans. Magn. 28 (1992) 2668.
[8] R.R. Katti, Proc. IEEE 91 (5) (2003) 687.
[9] A.M. Choukh, IEEE Trans. Magn. 32 (1996) 4526.
[10] N. Mao-Min Chen, G.L. Gharsallah, J. Gorman, Latimer, J. Appl. Phys. 69 (1991) 5631.
[11] P. Granberg, P. Isberg, E.B. Svedberg, B. Hjorvarsson, P. Nordblad, R. Wapping, J. Magn. Magn. Mater. 186 (1998) 154.
[12] B.D. Cullity, Elements of X-ray Diffraction, Addison-Wesley, London, 1978, p. 102.
[13] B.M. Clemens, Phys. Rev. B 33 (11) (1986) 7615.
[14] M. Abid, H. Ouahmane, H. Lassri, A. Khmou, R. Krishnan, J. Magn. Magn. Mater. 202 (1999) 335.
[15] K. Rook, J.O. Artman, IEEE Trans. Magn. 27 (1991) 5450.
[16] H. Puszkarski, Progr. Surf. Sci. 9 (1979) 191.
[17] N.K. Flevaris, R. Krishnan, J. Magn. Magn. Mater. 93 (1991) 439.
[18] C. Kittel, Phys. Rev. 110 (1958) 1295.
[19] A.H. Morrish, The Physical Principles of Magnetism, Wiley, New York, 1965, p. 588.
[20] J. Du, J. Wu, L.N. Tong, M. Lu, J.H. Du, M.H. Pan, H.R. Zhai, H. Xia, Phys. Stat. Sol. 167 (1998) 183.
[21] G.T. Rado, Phys. Rev. B 26 (1982) 295.
[22] L. Néel, J. Phys. Paris 15 (1954) 225.